

# Non-LTE effects on the lead and thorium abundance determinations for cool stars

L. Mashonkina<sup>1,2</sup>, A. Ryabtsev<sup>3</sup>, and A. Frebel<sup>4,5</sup>

<sup>1</sup> Universitäts-Sternwarte München, Scheinerstr. 1, D-81679 München, Germany  
e-mail: lyuda@usm.lmu.de

<sup>2</sup> Institute of Astronomy, Russian Academy of Sciences, RU-119017 Moscow, Russia  
e-mail: lima@inasan.ru

<sup>3</sup> Institute of Spectroscopy, Russian Academy of Sciences, 142190, Troitsk, Moscow region, Russia

<sup>4</sup> Massachusetts Institute of Technology, Kavli Institute for Astrophysics and Space Research, 77 Massachusetts Avenue, Cambridge, MA 02139, USA  
e-mail: afrebel@mit.edu

<sup>5</sup> Harvard-Smithsonian Center for Astrophysics, 60 Garden St, Cambridge, MA 02138, USA

Received / Accepted

## ABSTRACT

**Context.** Knowing accurate lead abundances of metal-poor stars provides constraints on the Pb production mechanisms in the early Galaxy. Accurately deriving thorium abundances permits a nucleo-chronometric age determination of the star.

**Aims.** We aim to improve the calculation of the Pb I and Th II lines in stellar atmospheres based on non-local thermodynamic equilibrium (non-LTE) line formation, and to evaluate the influence of departures from LTE on Pb and Th abundance determinations through a range of stellar parameters with variations of the metallicity from the solar value down to  $[\text{Fe}/\text{H}] = -3$ .

**Methods.** Comprehensive model atoms for Pb I and Th II are presented. We describe calculations of the Pb I energy levels and oscillator strengths.

**Results.** The main non-LTE mechanism for Pb I is the ultraviolet overionization. Non-LTE leads to systematically depleted total absorption in the Pb I lines and accordingly, positive abundance corrections. The departures from LTE grow with decreasing metallicity. Non-LTE removes the discrepancy between the solar photosphere and the meteoritic lead abundance. Using the semi-empirical Holweger & Müller (1974) model atmosphere, we determined the lead non-LTE abundance for the Sun to be  $\log \varepsilon_{\text{Pb},\odot} = 2.09$ . We revised the Pb and Eu abundances of the two strongly r-process enhanced stars CS 31082-001 and HE 1523-0901 and the Roederer et al. (2010) metal-poor stellar sample. Our new results provide strong evidence for universal Pb-to-Eu relative r-process yields during course of the evolution of the Galaxy. The stars in the  $-2.3 < [\text{Fe}/\text{H}] < -1.4$  metallicity range have, on average, 0.51 dex higher Pb/Eu abundance ratios compared with that of the strongly r-process enhanced stars. We conclude that the s-process production of lead started as early as the time when Galactic metallicity had grown to  $[\text{Fe}/\text{H}] = -2.3$ . The average Pb/Eu abundance ratio of the mildly metal-poor stars, with  $-1.4 \leq [\text{Fe}/\text{H}] \leq -0.59$ , is very close to the corresponding Solar System value, in line with the theoretical predictions of Travaglio et al. (2001) that AGB stars with  $[\text{Fe}/\text{H}] \simeq -1$  provided the largest contribution to the solar abundance of s-nuclei of lead. The departures from LTE for Th II are caused by the pumping transitions from the low-excitation levels, with  $E_{\text{exc}} < 1$  eV. Non-LTE leads to weakened Th II lines and positive abundance corrections. Overall, the abundance correction does not exceed 0.2 dex when collisions with H I atoms are taken into account in statistical equilibrium calculations.

**Key words.** Line: formation – Nuclear reactions, nucleosynthesis, abundances – Sun: abundances – Stars: abundances – Stars: atmospheres

## 1. Introduction

Lead ( $Z = 82$ ), thorium ( $Z = 90$ ), and uranium ( $Z = 92$ ) are the three heaviest elements observed in metal-poor (MP) stars, with  $[\text{Fe}/\text{H}]^1 < -1$ . Only one detection of bismuth ( $Z = 83$ ) has ever been made in an MP star (Ivans et al. 2005), because the only suitable line, Bi I 3067 Å, lies in a very crowded spectral region in the near-UV that is difficult to access. All nuclei between  $^{209}\text{Bi}$  and  $^{244}\text{Pu}$  and which exist in nature, are radioactive. Among them, only Th and U have long-lived isotopes with half-lives longer than 1 Gyr,  $t_{1/2}(^{232}\text{Th}) \simeq 14$  Gyr and  $t_{1/2}(^{238}\text{U}) \simeq 4.5$  Gyr, and can be detected in spectra of MP stars.

The knowledge of stellar Pb abundances provides a better understanding of the production mechanisms of lead during the evolution of the Galaxy. Lead is produced by two neutron-capture processes on different timescales, i.e., in the slow (s) process occurring during thermally pulsing asymptotic giant branch (AGB) phase of intermediate-mass ( $2-8 M_{\odot}$ ) stars (see for example, Gallino et al. 1998) and the rapid (r) process. The astrophysical site at which the r-process operates has not yet been identified. Given that the heavy elements, such as Ba and Eu, are detected in very metal-poor (old) stars, supernovae with progenitors of  $8-10 M_{\odot}$  are the most promising candidates for r-process enrichment in the early Galaxy. See, for example, the pioneering review of Hillebrandt (1978) and also Cowan & Thielemann (2004) for further discussion on the r-process. Theoretical studies of the s-process showed that in low-metallicity environment, heavy s-nuclei like those of Pb are more efficiently produced

Send offprint requests to: L. Mashonkina; e-mail: lima@inasan.ru

<sup>1</sup> In the classical notation, where  $[\text{X}/\text{H}] = \log(N_{\text{X}}/N_{\text{H}})_{\text{star}} - \log(N_{\text{X}}/N_{\text{H}})_{\text{sun}}$ .

compared to lighter nuclei due to the higher ratio of free neutrons to Fe-peak seeds, and also due to an extended period of s-process nucleosynthesis (Gallino et al. 1998, Travaglio et al. 2001). It was predicted that the AGB stars with  $[\text{Fe}/\text{H}] \simeq -1$  made the greatest contribution to the solar abundance of s-nuclei of lead. According to Travaglio et al. (2001), the s-process fraction of the solar Pb amounts to 81 %.

The largest data set on lead abundances of MP stars was compiled by Roederer et al. (2010). They found that the stellar Pb/Eu abundance ratios form a plateau in the metallicity range  $-2.3 < [\text{Fe}/\text{H}] < -1.4$ , and Pb/Eu grows at higher metallicity. The increase of Pb/Eu at  $[\text{Fe}/\text{H}] > -1.4$  suggests a growing contribution to the stellar lead abundance from the s-process opening in AGB stars. Roederer et al. (2010) concluded that s-process material was not widely dispersed until the Galactic metallicity grew considerably, as high as  $[\text{Fe}/\text{H}] = -1.4$ . This also means that lead in stars with lower metallicity should be of pure r-process origin. It is worth noting that despite the large scatter in the Pb/Eu abundance ratios in the Roederer et al. (2010) stars with  $-2.3 < [\text{Fe}/\text{H}] < -1.4$ , the ratios are, on average, 0.85 dex higher compared with the corresponding value in the strongly r-process enhanced star CS 31082-001 (Plez et al. 2004). With  $[\text{Eu}/\text{Fe}] = 1.6$  (Hill et al. 2002), this star experienced enrichment from, probably, a single r-process source. Following the suggestion of Christlieb et al. (2004), we hereafter refer to stars having  $[\text{Eu}/\text{Fe}] > +1$  and  $[\text{Ba}/\text{Eu}] < 0$  as r-II stars. The heavy element abundance ratios of each r-II star are expected to reflect the relative yields of the r-process. What can be the reason of the large discrepancy in Pb/Eu between CS 31082-001 and the  $-2.3 < [\text{Fe}/\text{H}] < -1.4$  stars?

In the visual spectra of MP stars, lead is represented by the lines of Pb I. Due to a relatively low ionization energy of 7.43 eV, lead is mostly ionized in the stellar atmospheres with effective temperature hotter than  $T_{\text{eff}} = 4000$  K, and the number density of neutral lead can easily deviate from the thermodynamic equilibrium (TE) population, owing to deviations of the mean intensity of ionizing radiation from the Planck function. All previous stellar Pb analyses have been made under the local thermodynamic equilibrium (LTE) assumption, and the obtained results should be checked for any departures from LTE.

The detection of thorium permits, in principle, a nucleochronometric age estimate of the star by comparing the observed Th-to-stable neutron-capture element-abundance ratios with the corresponding initial values provided by the r-process event just prior to the time when the star was born (see, for example, Sneden et al. 1996, Cayrel et al. 2001, Frebel et al. 2007). Given that the half-life of  $^{232}\text{Th}$  is long, stellar thorium has to be measured very precisely, with abundance errors of no more than 0.05 dex, to provide less than 2.3 Gyr uncertainty in the star's age.

This study aimed to improve the calculation of the Pb I and Th II lines in stellar atmospheres based on the non-local thermodynamic equilibrium (non-LTE) line formation and to evaluate systematic abundance errors caused by the simplified LTE line formation treatment. We constructed, for the first time, model atoms for Pb I and Th II. The non-LTE method and the departures from LTE for Pb I are described in Sect. 2. Our theoretical results were used to determine the solar lead abundance (Sect. 3) and to revise the Pb abundances of the Roederer et al. (2010) stellar sample (Sect. 4). Having added the r-II star HE 1523-0901 (Frebel et al. 2007), we found that the Pb/Eu abundance ratios of the two r-II stars are well reproduced by the waiting-point r-process model as presented by Roederer et al. (2009), while an additional source of lead, most probably, the s-process in AGB

stars, is needed to explain the Pb abundances of the stars with  $[\text{Fe}/\text{H}] > -2.3$ . The non-LTE calculations for Th II are presented in Sect. 5. Our conclusions are given in Sect. 6.

## 2. Non-LTE calculations for Pb I

To solve the coupled radiative transfer and statistical equilibrium (SE) equations, we used a revised version of the DETAIL program (Butler & Giddings 1985) based on the accelerated lambda iteration (ALI) method as described by Rybicki & Hummer (1991, 1992). The update was presented by Mashonkina et al. (2011). The non-LTE calculations were performed with the MARCS model atmospheres (Gustafsson et al. 2008)<sup>2</sup>.

### 2.1. Pb I atomic structure calculations

The atomic structure of neutral lead has been well studied with laboratory measurements. The ground level of Pb I is  $6s^2 6p^2 \ ^3P_0$ , and the ionization of the 6p electron gives the ionic core (Pb II)  $6s^2 6p$ , which splits into two levels,  $^2P_{1/2}^\circ$  (lower ionization limit  $59819.57 \text{ cm}^{-1}$ ) and  $^2P_{3/2}^\circ$  (upper ionization limit  $73900.64 \text{ cm}^{-1}$ ) in the LS coupling scheme. The Pb I energy structure more closely approaches the *JJ* than the *LS* coupling. Thus, the ground configuration  $6s^2 6p^2$  possesses 5 energy levels which are designated as  $(1/2, 1/2)_0$ ,  $(1/2, 3/2)_1$ ,  $(3/2, 1/2)_2$ ,  $(3/2, 3/2)_2$ , and  $(3/2, 3/2)_0$ . The energy separation between the  $6s^2 6p^2$  levels is remarkably large, for example, the second and the fifth level have an excitation energy of  $E_{\text{exc}} = 0.97 \text{ eV}$  and  $3.65 \text{ eV}$ , respectively. Almost all the remaining known energy levels of Pb I belong to the  $6s^2 6pnl$  electronic configurations. Hereafter,  $6s^2$  is omitted in the configuration designations.

The early data on the Pb I energy levels obtained before 1958 were summarized by Moore (1958). After that, the analysis was greatly extended using classical emission (Wood & Andrew 1968) and absorption (Brown et al. 1977) spectroscopy as well as selective laser excitation (the papers relevant to our study are cited below). The measurements of long Rydberg series terminating on the first ionization limit provided many odd parity levels of the 6pns and 6pnd (Brown et al. 1977, up to  $n = 59$  and  $n = 77$ , respectively), and 6png ( $n = 5-9$  in Wood & Andrew (1968) and  $n = 21-47$  in Dembczyński et al. (1994)) configurations. Even parity levels of the 6pnp ( $n = 7-60$ ) and 6pnf ( $n = 5-56$ ) configurations were measured by Hasegawa & Suzuki (1996) a total of 205 energy levels with a total angular momentum  $J = 0, 1$ , and  $2$ . Information on several hundred autoionizing levels above the first ionization limit is available (see Ahad et al. 2005, and references therein).

The data on transition probabilities in Pb I available in the literature (Biémont et al. 2000, Fuhr & Wiese 1992) are incomplete, and we rely on oscillator strengths computed in this study. The atomic structure of Pb I was calculated using the Cowan code (Cowan 1981). The 22 even parity interacting configurations  $6p^2 + 6pnp$  ( $7 \leq n \leq 15$ ) +  $6pnf$  ( $5 \leq n \leq 12$ ) +  $6p6h + 6p7h + 6s6p^2 7s + 6p^4$  were included in the energy matrix, while the odd set was restricted to 24 configurations, i.e.,  $6pns$  ( $7 \leq n \leq 12$ ) +  $6pnd$  ( $6 \leq n \leq 12$ ) +  $6png$  ( $5 \leq n \leq 12$ ) +  $6sp^2 7p + 6s6p^3 + 5d^9 6s^2 6p^3$ . The calculations generally follow the scheme used by Biémont et al. (2000). During the fitting of the calculated energy levels to the experimental ones, the number of varying energy parameters was restricted as much as possible. All the parameters describing the configurations in the 6pnl series for different

<sup>2</sup> <http://marcs.astro.uu.se>

n were varied collectively keeping the ratios of the corresponding *ab initio* values. The exchange Slater integrals  $G^k$  within the configurations were also varied in a similar way. The electrostatic parameters including the configuration interaction parameters, which were not optimized in the fitting procedure, were scaled down by a factor of 0.80, while the spin-orbit integrals were fixed at their *ab initio* values. As a result, the 67 even parity levels were described by the 25 parameters with a standard deviation of  $73 \text{ cm}^{-1}$  and the 51 odd parity levels by 21 parameters with a standard deviation of  $74 \text{ cm}^{-1}$ . Our atomic structure calculations complemented the system of known energy levels in the region above  $6.87 \text{ eV}$  with the 20 even parity levels of the  $6\text{pnf}$  ( $n = 9-12$ ,  $J = 3$  and  $4$ ) and  $6\text{pnh}$  ( $n = 6, 7$ ) configurations and 29 odd parity levels belonging mostly to the  $6\text{png}$  ( $n = 5-12$ ) configurations.

The wavefunctions obtained after the fitting of energy levels were used for the calculations of transition probabilities. The dipole transition integrals for all transitions were kept at *ab initio* Hartree-Fock values. The accuracy of our calculations was estimated by the comparison with the experimental data for common levels. Figure 1 shows that the difference in lifetime between our calculations and the measurements of Biémont et al. (2000) is mostly within 75 %, with the only outlier being the measured to calculated lifetime ratio of about 2.3. On average, the predicted lifetimes approach to the measured values. It should be noted that the lifetimes of the highest  $6\text{pnd}$  levels with  $J = 2$  are critically dependent on a position of strongly interacting  $6s6p^3^5S_2^\circ$  level. It seems that the only  $^3P_1^\circ$  level of the  $6s6p^3$  configuration is firmly located at  $E_{\text{exc}} = 85870 \text{ cm}^{-1}$  (Krause et al. 1986, Müller et al. 1990). Dembczyński et al. (1994) estimated the position of the  $6s6p^3^3D_1^\circ$  level at  $E_{\text{exc}} = 68943 \text{ cm}^{-1}$  from analysis of the interactions in the  $6\text{pns}$  and  $6\text{pnd}$  series. They also established that “the state  $6s6p^3^5S_2^\circ$  does not occur as a dominant component in any of the electronic levels but it mixed into many odd levels”. Its unperturbed value should be around  $59300 \text{ cm}^{-1}$ . To predict the levels of the  $6s6p^3$  configuration, the same scaling of *ab initio* values was applied to the parameters within the  $6p^3$  subshell as that for the  $6s^26p^2$  configuration. The average energy and the  $G^1(6s,6p)$  parameter were adjusted to fit the energies of the  $^3P_1^\circ$  and  $^3D_1^\circ$  levels. The energy of the  $6s6p^3^5S_2^\circ$  level appeared to be  $58700 \text{ cm}^{-1}$ , in quite good agreement with the estimates of Dembczyński et al. (1994). Similar consistency between theory and measurements was found for the even parity  $6\text{pnp}$  ( $7 \leq n \leq 14$ ) and  $6\text{pnf}$  ( $6 \leq n \leq 8$ ) levels when using the measured lifetimes of Li et al. (2001).

Figure 1 shows also the measured to calculated lifetime ratios from the calculations of Biémont et al. (2000), who took into account the core polarization effect that is expected to give rise to the precision of the predicted lifetimes. As can be seen, our results obtained without taking into account the core polarization agree very well with the calculations of Biémont et al. (2000). Therefore, *gf*-values calculated in this study are expected to have the same accuracy as the values in Biémont et al. (2000) for all the transitions in Pb I.

## 2.2. Lead model atom

**Energy levels.** To construct the model atom, we used all the measured and predicted levels in Pb I. They are shown in Fig. 2. The high-excitation ( $E_{\text{exc}} \geq 6.04 \text{ eV}$ ) levels with common parity and energy separation of smaller than  $0.01 \text{ eV}$  were combined into a single level. The final model atom is fairly complete. It includes

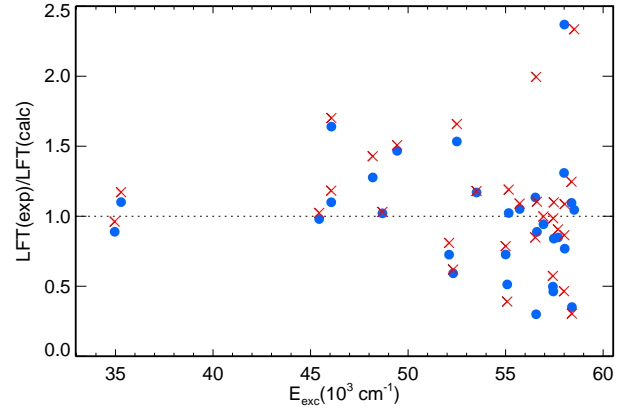


**Fig. 1.** Measured (Biémont et al. 2000) to calculated Pb I lifetime ratios for the  $6\text{pns}$  ( $7 \leq n \leq 12$ ) and  $6\text{pnd}$  ( $6 \leq n \leq 13$ ) levels, mostly with  $J = 1$  and  $2$ . Open circles and crosses correspond to our and the Biémont et al. (2000) calculations, respectively.

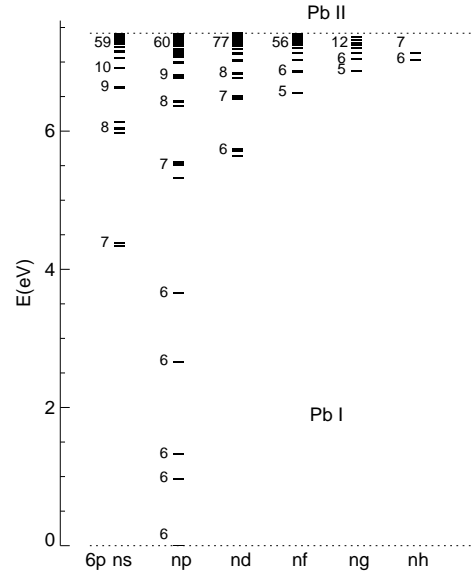


**Fig. 2.** Measured and predicted energy levels of Pb I that form our final Pb model atom.

97 levels of Pb I and the ground state  $6s^26p^2P_{1/2}^\circ$  of Pb II. The second sublevel of the ground term,  $^2P_{3/2}^\circ$  ( $E_{\text{exc}} = 1.75 \text{ eV}$ ), was taken into account only in the number conservation equation. The excited electronic configurations of Pb II produce levels with an excitation energy of more than  $7.2 \text{ eV}$ , and were thus ignored.

**Radiative rates.** For 141 transitions in Pb I that connect the  $6p^2$  and  $6p7p$  levels to the  $6\text{pns}$  and  $6\text{pnd}$  ( $n \leq 13$ ) ones, we employed accurate *gf*-values based on measured natural radiative lifetimes and theoretical branching ratios from Biémont et al. (2000) and Fuhr & Wiese (1992). For the remaining majority of transitions, we used oscillator strengths computed in this study. In total, 1954 radiative bound-bound ( $b - b$ ) transitions in Pb I were included in our SE calculations.

For the Pb I ground state, we applied the photoionization cross-sections  $\sigma_{\text{ph}}$  measured by Heppinstall & Marr (1969) from



the ionization threshold at 1671 to 1470 Å. For the remaining levels,  $\sigma_{\text{ph}}$  were computed using the hydrogen approximation formula with  $n = n_{\text{eff}}$ , where  $n_{\text{eff}} = Z \sqrt{\chi_{\text{H}}/\chi_i}$  is the effective principal quantum number for the level with the ionization energy  $\chi_i$ . Here,  $Z = 1$  and  $\chi_{\text{H}}$  is the hydrogen ionization energy. Such a choice was justified by the comparison of the experimental threshold cross-section  $\sigma_{\text{thr,exp}} = 10 \text{ Mb}$  for the Pb I ground state with the cross-sections calculated with various  $n$ . The use of  $n = 6$  results in the too low hydrogen approximation cross-section  $\sigma_{\text{thr,hyd}} = 0.0007 \text{ Mb}$ . With  $n_{\text{eff}} = 1.35$ , we computed  $\sigma_{\text{thr,hyd}} = 1.3 \text{ Mb}$ , which is much closer to the experimental data, although it is about a factor of 10 lower.

**Collisional rates.** All levels in our model atom are coupled via collisional excitation and ionization by electrons and by neutral hydrogen atoms. The calculations of collisional rates rely on theoretical approximations. For electron-impact excitation, we used the formula of van Regemorter (1962) for the allowed transitions and we assumed that the effective collision strength  $\Upsilon = 1$  for the forbidden transitions. Electron-impact ionization cross-sections were computed according to Drawin (1961).

For collisions with H I atoms, we employed the classical Drawin formula as described by Steenbock & Holweger (1984). Over the past few decades, this formula has been criticized for significantly overestimating the collision rates (see Barklem et al. 2011, and references therein). At the same time, the need for a thermalizing process not involving electrons in the atmospheres of, in particular, very metal-poor stars, was indicated by many non-LTE spectral line formation studies (see Mashonkina et al. 2011, and references therein). Because no accurate calculations of either inelastic collisions of lead with neutral hydrogen atoms or other types of processes are available, we simulate an additional source of thermalization in the atmospheres of cool stars by using parametrized H I collisions. The Drawin formula can only be applied to allowed  $b - b$  and  $b - f$  transitions. For the forbidden transitions, a simple relation between hydrogen and electron collision rates,  $C_{\text{H}} = C_e \sqrt{(m_e/m_{\text{H}})N_{\text{H}}/N_e}$ , was used following Takeda (1995). The SE calculations were performed with various efficiencies of collisions with H I atoms by applying a scaling factor of  $S_{\text{H}} = 0$  (no hydrogen collisions), 0.1, and 1.

We discuss below the effects of the uncertainty in the adopted photoionization cross-sections and collisional rates on our final results.

### 2.3. Departures from LTE for Pb I

We first inspect the statistical equilibrium of lead in the two model atmospheres representing the solar atmosphere, with  $T_{\text{eff}}/\log g/[\text{Fe}/\text{H}] = 5780/4.44/0$ , and the atmosphere of a typical very metal-poor (VMP) cool giant (4500/1.0/−3) from the calculations with  $S_{\text{H}} = 0.1$ . The departure coefficients,  $b_i = n_i^{\text{NLTE}}/n_i^{\text{LTE}}$ , for the Pb I and Pb II levels are shown in Fig. 3. Here,  $n_i^{\text{NLTE}}$  and  $n_i^{\text{LTE}}$  are the statistical equilibrium and TE number densities, respectively. In these computations, the Pb abundance was adopted at  $\log \varepsilon_{\text{Pb}} = 1.92$  in the solar model and at  $\log \varepsilon_{\text{Pb}} = -0.08$  ([Pb/Fe] = +1) in the VMP model. In each model, lead is almost completely ionized, such that the fraction of Pb I nowhere exceeds 4% in the solar atmosphere and 0.6% in the cool VMP atmosphere. This explains why the non-LTE mechanisms for Pb I are similar in the two models. We summarize our findings as follows.

1. In the atmosphere outside  $\log \tau_{5000} = +0.2$  and  $+0.5$  for the solar and VMP models, respectively, the most populated  $6p^2$  lev-

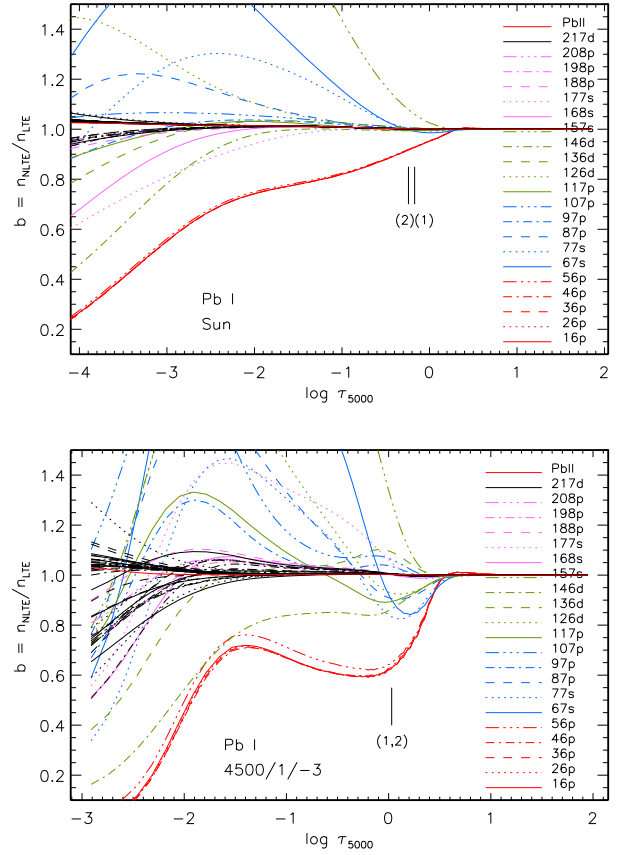


**Fig. 3.** Departure coefficients,  $b$ , for the lowest 60 levels of Pb I and the ground state of Pb II as a function of  $\log \tau_{5000}$  in the model atmospheres 5780/4.44/0 (top panel) and 4500/1.0/−3 (bottom panel). The first 21 levels are quoted in the right part of each panel. For all the higher excitation levels, their behaviour is very similar to that of the 188p to 217d levels, with  $b \approx 1$  in the solar and VMP models inside  $\log \tau_{5000} = -3$  and  $-1$ , respectively.  $S_{\text{H}} = 0.1$  was used throughout. The vertical lines indicate the locations of line core formation depths for Pb I 4057 (1) and 3683 Å (2). See text for more details.

els of Pb I are underpopulated relative to their TE number densities and they are close together. The main non-LTE mechanism is the ultraviolet (UV) overionization caused by superthermal radiation of a non-local origin below the thresholds at  $\lambda_{\text{thr}} = 1923$ , 2033, and 2606 Å for the three excited  $6p^2$  levels.

2. The populations of the  $6p^2$  levels labeled in the model atom as 67s and 77s are controlled by the two mechanisms. The UV overionization ( $\lambda_{\text{thr}} = 4022$  and  $4076 \text{ Å}$ ) tends to drain the populations far inside the atmosphere. The competing process is radiative pumping of the strong  $6p^2 - 6p^2$  transitions ( $(1/2, 1/2)_0 - (1/2, 1/2)_1$  (16p - 77s in our denotations, which produces the line at 2833 Å),  $(1/2, 3/2)_1 - (1/2, 1/2)_0$  (26p - 67s, 3683 Å), and  $(1/2, 3/2)_1 - (1/2, 1/2)_1$  (26p - 77s, 3639 Å) by the ultraviolet  $J_{\nu} - B_{\nu}(T_e)$  excess radiation which tends to produce enhanced excitation of the upper levels in the atmospheric layers, where the line wing optical depth drops below 1. The net effect is that the 67s and 77s levels are underpopulated far inside the atmosphere, at  $\log \tau_{5000} = -0.7$  to  $+0.2$  and  $-0.3$  to  $+0.2$  in the models 4500/1.0/−3 and 5780/4.44/0, respectively, and they are overpopulated in the higher layers. No process seems to com-

pete with radiative pumping of the 26p - 157s (2476 Å) and 36p - 157s (2663 Å) transitions resulting in strong overpopulation of the upper level in the atmosphere outside  $\log \tau_{5000} = +0.2$ .

3. The overpopulation of the 6p7s levels is redistributed to the 6p7p levels through inelastic collisions.

4. All the high-excitation levels with  $E_{\text{exc}} \geq 6.1$  eV (starting from the 18th level in the model atom) couple thermally to the Pb II ground state.

5. Pb II represents the state in which the majority of the element exists and it preserves, therefore, the TE population.

The formation depth has been specified as the depth where  $\tau_{\nu} \lambda_{\nu}^{1/2} = 1$ , following Mihalas (1978). Here,  $\lambda_{\nu}$  is the ratio of the thermal to total absorption coefficient. Everywhere in the solar atmosphere,  $\lambda_{\nu} \approx 1$ , irrespective of the frequency point. In the cool VMP model,  $\lambda_{\nu} < 1$  due to significant contribution of Rayleigh scattering to the total opacity. For example, at the depth point  $\log \tau_{5000} = 0$ ,  $\lambda_{\nu} \approx 0.7$  at 4057 Å and it decreases towards shorter wavelengths. Even lower  $\lambda_{\nu}$  values are obtained in the higher atmospheric layers.

The two lines, Pb I 4057 Å ( $6p^2 (1/2, 3/2)_2 - 6p7s (1/2, 1/2)_1$ ) denoted as 36p - 77s in our model atom and 3683 Å ( $6p^2 (1/2, 3/2)_1 - 6p7s (1/2, 1/2)_0$ ) denoted as 26p - 67s), and, in many cases, only one of them are used in stellar Pb abundance analyses. In each model, non-LTE leads to a weakening of the Pb I lines compared to their LTE strengths and thus positive non-LTE abundance corrections. This is due to overionization ( $b_l < 1$ ) and also owing to the line source function  $S_{lu} \approx b_u/b_l B_{\nu}$  rises ( $b_u > b_l$ ) being above the Planck function  $B_{\nu}$  in the line-formation layers (Fig. 3). Here,  $b_u$  and  $b_l$  are the departure coefficients of the upper and lower levels, respectively. We found that the departures from LTE are significantly larger in the VMP model compared to the solar one. The non-LTE abundance correction,  $\Delta_{\text{NLTE}} = \log \varepsilon_{\text{NLTE}} - \log \varepsilon_{\text{LTE}}$ , decreases from +0.21 down to +0.09 dex for Pb I 3683 Å in the solar model when  $S_H$  moves from 0 to 1. Similar values, +0.19 and +0.11 dex, were obtained for Pb I 4057 Å. In the 4500/1/-3 model,  $\Delta_{\text{NLTE}}(\text{Pb I } 4057 \text{ Å}) = +0.49$  and +0.38 dex when  $S_H = 0$  and 1, respectively.

Using  $S_H = 0.1$ , we computed  $\Delta_{\text{NLTE}}$  for the grid of model atmospheres characteristic of the Galactic halo stars. Table 1 presents the resulting values for Pb I 4057 Å. It can be seen that the non-LTE correction grows toward lower metallicity from  $\Delta_{\text{NLTE}} = 0.16$  dex in the solar model up to  $\Delta_{\text{NLTE}} = 0.62$  dex in the 5000/1.50/-3 one. For a given metallicity,  $\Delta_{\text{NLTE}}$  increases with increasing  $T_{\text{eff}}$  and decreasing  $\log g$ .

Besides different prescriptions of the collisions with hydrogen atoms, two different test calculations were performed for the 4500/1/-3 model to assess the influence of crucial atomic data on final results. Here, we used  $S_H = 0.1$ . First, we varied photoionization cross-sections by employing the principal quantum number  $n$  instead of  $n_{\text{eff}}$  in the hydrogen approximation formula. For the 6p<sup>2</sup> and 6p7s levels, this resulted in the reduction of  $\sigma_{ph}$  by a factor of 150 to 70. However, the effect on  $\Delta_{\text{NLTE}}$  for Pb I 4057 Å was found to be minor, of less than 0.01 dex, because the departures from LTE for this line are controlled by the  $b - b$  radiative transitions between the 6p<sup>2</sup> and 6p7s levels.

Second, we checked the atomic model, where H I collisions were taken into account for the allowed transitions, but were neglected for the forbidden ones. As expected, this resulted in strengthening the departures from LTE. For Pb I 4057 Å,  $\Delta_{\text{NLTE}}$  grew from 0.41 dex up to 0.53 dex. Thus, poor knowledge of collisions with H I atoms is the main source of the uncertainty in the calculated non-LTE abundance corrections for the Pb I lines.

**Table 1.** Non-LTE abundance corrections (dex) for the Pb I 4057 Å and Eu II 4129 Å lines from the calculations with  $S_H = 0.1$ .

$T_{\text{eff}}$	$\log g$	[Fe/H]	$\Delta_{\text{NLTE}}$	
			Pb I	Eu II
5780	4.44	0	0.16	0.03
		[Pb/Fe] = 0.5 <sup>1</sup> , [Eu/Fe] = 0.7 <sup>1</sup>		
4750	1.5	-1	0.26	0.06
5000	3.0	-1	0.32	0.06
5000	4.0	-1	0.28	0.05
5000	4.5	-1	0.22	0.04
5500	4.0	-1	0.31	0.05
5500	4.5	-1	0.27	0.05
4000	0.0	-2	0.38	0.12
4000	0.5	-2	0.32	0.08
4250	0.5	-2	0.33	0.07
4250	1.0	-2	0.30	0.06
4500	1.0	-2	0.30	0.06
4500	1.5	-2	0.32	0.06
4750	1.5	-2	0.37	0.07
4750	2.0	-2	0.39	0.07
5250	2.5	-2	0.52	0.10
		[Pb/Fe] = 1.0 <sup>1</sup> , [Eu/Fe] = 1.8 <sup>1</sup>		
4500	1.0	-3	0.41	0.04
4500	1.5	-3	0.42	0.04
4750	1.0	-3	0.49	0.06
4750	1.5	-3	0.53	0.06
5000	1.5	-3	0.62	0.07

<sup>1</sup> Abundances used in non-LTE calculations.

### 3. Solar lead abundance

As a test and first application of the Pb I model atom, we determined the lead abundance for the Sun. We used solar central intensity observations taken from the Kitt Peak Solar Atlas of Brault et al. (1972). The only useful line of Pb I at 3683.46 Å lies in a rather crowded spectral region, and the element abundance was derived applying the line-profile fitting method with the SIU program (Reetz 1991). We employed the semi-empirical solar model atmosphere of Holweger & Mueller (1974, hereafter, HM74) and the theoretical MARCS model (Gustafsson et al. 2008) with  $T_{\text{eff}} = 5780$  K and  $\log g = 4.44$ . A depth-independent microturbulence of  $0.9 \text{ km s}^{-1}$  was adopted.

The continuum level in the spectral range 3678-3688 Å was fixed using an atomic line list from the VALD database (Kupka et al. 1999) and a molecular line list from Kurucz (1994). Our synthetic intensity profiles were convolved with a radial-tangential macroturbulence profile of  $V_{\text{mac}} = 2.5 \text{ km s}^{-1}$ . Figure 4 illustrates the fit of the 3683 Å blend, in particular, Pb I 3683.46 Å and the strong Fe I 3683.612 and 3683.629 Å lines. For Pb I 3683.46 Å,  $\log gf = -0.52$  (Biémont et al. 2000) was employed throughout.

Under the LTE assumption, we obtained  $\log \varepsilon_{\text{Pb,LTE}} = 1.96$  with the HM74 model and  $\log \varepsilon_{\text{Pb,LTE}} = 1.85$  with the solar MARCS model. It should be stressed that the solar photosphere lead LTE abundance is lower than the meteoritic one  $\log \varepsilon_{\text{Pb,met}} = 2.04 \pm 0.03$  (Asplund et al. 2009) and  $2.06 \pm 0.03$  (Lodders et al. 2009), independent of the applied model atmosphere. The two recent LTE determinations yielded  $\log \varepsilon_{\text{Pb,LTE}} = 1.75 \pm 0.10$  based on the theoretical 3D model (Asplund et al. 2009) and  $2.00 \pm 0.06$  based on the HM74 model (Lodders et al. 2009).

We found that non-LTE decreases the discrepancy between the solar photosphere and meteoritic Pb abundance. When using

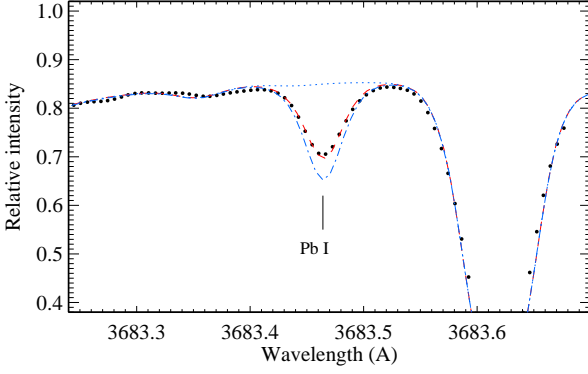


**Fig. 4.** Synthetic non-LTE ( $S_H = 0.1$ , dashed curve) and LTE (dash-dotted curve) disk-center intensity profiles of Pb I 3683.46 Å computed with the HM74 model atmosphere and  $\log \varepsilon_{\text{Pb}} = 2.09$  compared with the observed spectrum of the Brault et al. (1972) solar atlas (bold dots). Dotted curve corresponds to the atmosphere without lead.

the HM74 model, the non-LTE abundances amount to  $\log \varepsilon_{\text{Pb}} = 2.12, 2.09$ , and  $2.03$  from the calculations with  $S_H = 0, 0.1$ , and  $1$ , respectively. Figure 4 shows the best non-LTE fit for  $S_H = 0.1$ . For the solar MARCS model, the non-LTE abundances are  $2.00, 1.97$ , and  $1.92$  depending on the used  $S_H$  value, i.e., for  $0, 0.1$ , and  $1$ , respectively. We note that, in all cases, the non-LTE correction calculated for the emergent intensity spectrum is smaller than that for the flux spectrum. This is because the disk-center radiation emerges from deeper layers, where the departures from LTE are weaker. From the analysis of the Pb I 3683 Å line alone we can not decide about the efficiency of poorly known inelastic collisions with H I atoms in SE calculations, and we choose  $S_H = 0.1$  based on our empirical estimates for Ca I-Ca II and Fe I-Fe II (Mashonkina et al. 2007, 2011). Thus, our final solar lead abundance is  $\log \varepsilon_{\text{Pb,NLTE}} = 2.09$  with the HM74 model atmosphere and  $\log \varepsilon_{\text{Pb,NLTE}} = 1.97$  with the solar MARCS model.

#### 4. Constraints on the Pb production mechanisms in the early Galaxy

In this section, we revise the Pb abundances of metal-poor stars available in the literature and investigate the metallicity behaviour of Pb/Eu abundance ratio. This ratio is particularly sensitive to whether the production of lead occurred in a pure r-process or whether there was a non-negligible s-process contribution. The r-nuclei of lead are produced through several decay channels. At the time when the r-process event stops (likely after a few seconds), there is the direct  $\beta^-$  decay of very neutron-rich isobaric nuclei with  $A = 206 - 208$  to  $^{206}\text{Pb}$ ,  $^{207}\text{Pb}$ , and  $^{208}\text{Pb}$ . Then there is the  $\alpha$ - and  $\beta$ -decay of nuclei with  $210 \leq A \leq 231$  and  $A = 234$  back to Pb, which operates shortly after the termination of the r-process, within few million years. And finally the radioactive decay of the long-lived Th and U isotopes produced Pb over the course of almost the age of the Galaxy. As stressed by Roederer et al. (2009), no Pb isotopes can be measured individually due to the relatively small isotope shifts ( $\leq 0.02 - 0.03$  Å) and overall weakness of the Pb I lines.

Hence, for the total elemental abundances, the classical waiting-point (WP) r-process model of Kratz et al. (2007) predicts  $\log \varepsilon_{\text{r},0}(\text{Pb}/\text{Eu}) = 0.61$  in a newly born star and  $\log \varepsilon_{\text{r},13}(\text{Pb}/\text{Eu}) = 0.70$  in a 13 Gyr old star (Roederer et al.

2009). Another estimate of a pure r-process production ratio can be obtained using the Solar r-residuals. With an s-process contribution to the solar Pb of 81 % (Travaglio et al. 2001)<sup>3</sup> and to the solar Eu of 6 % (Travaglio et al. 1999), we computed the Solar System r-process ratio  $\log \varepsilon_{\text{SSr}}(\text{Pb}/\text{Eu}) = 0.82$ . When computing s-fractions, Travaglio et al. (1999, 2001) used the meteoritic isotope abundances from Anders & Grevesse (1989). For comparison, the ratio of the meteoritic total abundances is  $\log \varepsilon_{\text{met}}(\text{Pb}/\text{Eu}) = 1.51$  and  $1.53$  according to Anders & Grevesse (1989) and Lodders et al. (2009), respectively.

The largest data set on stellar Pb abundances was compiled by Roederer et al. (2010). Their data are based on the analysis of Pb I 4057 Å. Before correcting these abundances, we excluded all stars with only upper limits for Pb abundance, the carbon-enhanced stars with  $[\text{C}/\text{Fe}] > 0.3$ , and also VMP stars enriched in s-process material, with  $\log \varepsilon(\text{Pb}/\text{Eu}) \geq +1.8$  at  $[\text{Fe}/\text{H}] < -2$  (see small blue “x” in their Fig. 3) from the Roederer et al. (2010) sample. Regarding obtaining carbon abundances for these stars to check upon, we also relied on the Simmerer et al. (2004) study, which was used by Roederer et al. (2010) to compile most of their stellar sample. In total, 49 stars were selected in the  $-2.26 \leq [\text{Fe}/\text{H}] < -0.59$  metallicity range. We added to them the two r-II stars, i.e., CS 31082-001 (Hill et al. 2002, Plez et al. 2004) and HE 1523-0901 (Frebel et al. 2007, 2012, in preparation), and also the halo star HD 29907 from Sitnova & Mashonkina (2011). The stars used are listed in Table 2 with stellar parameters and LTE element abundances taken from the cited papers and with non-LTE abundance corrections obtained in this study. The non-LTE calculations were performed with the MARCS model atmospheres (Gustafsson et al. 2008). Where necessary, the MARCS model structures were interpolated for given  $T_{\text{eff}}$ ,  $\log g$ , and  $[\text{Fe}/\text{H}]$  using a FORTRAN-based routine written by Thomas Masseron (<http://marcs.astro.uu.se/software.php>). For each star, the SE calculations were performed using its given LTE element abundance.

For self-consistency, we also revised the europium abundances of the stars in our sample. The non-LTE calculations for Eu II were performed using the method treated by Mashonkina & Gehren (2000). Everywhere,  $S_H = 0.1$  was adopted. In the stellar parameter range with which we are concerned, non-LTE leads to weakened Eu II lines and positive abundance corrections. We computed  $\Delta_{\text{NLTE}}$  for the seven lines, i.e., Eu II 3724, 3819, 4129, and 4205 Å with  $E_{\text{exc}} = 0$  and Eu II 3907, 4435, and 4522 Å with  $E_{\text{exc}} = 0.21$  eV. Table 1 presents the resulting values for Eu II 4129 Å in the grid of model atmospheres characteristic of the Galactic halo stars. Table 2 does the same for the stars in our sample. For each line,  $\Delta_{\text{NLTE}}$  grows toward lower metallicity and lower surface gravity, although, it is overall small and does not exceed 0.17 dex for different lines. For example,  $\Delta_{\text{NLTE}}$  ranges between 0.02 and 0.06 dex for different lines in the 5600/3.75/-0.59 model, between 0.04 and 0.14 dex in the 4825/1.5/-2.9 model, and between 0.05 and 0.17 dex in the 4050/0.0/-2.08 model. For each model atmosphere,  $\Delta_{\text{NLTE}}$  of Eu II 4129 Å turned out to well represent the mean non-LTE correction from all the computed lines. For a given star, we used it as the mean non-LTE correction and applied it to the observed europium LTE abundance.

<sup>3</sup> These authors actually indicated 91 %. However, using s-fractions of 90, 60, 77, and 89 % for the  $^{204}\text{Pb}$ ,  $^{206}\text{Pb}$ ,  $^{207}\text{Pb}$ , and  $^{208}\text{Pb}$  isotopes, respectively, from their Table 3, we calculated an s-fraction of 81 % for the total lead abundance.



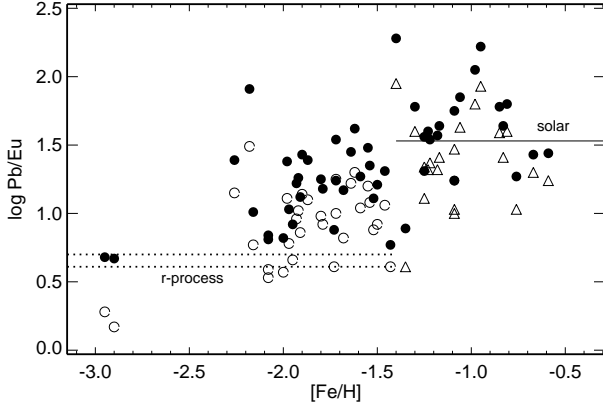


**Fig. 5.** Stellar non-LTE (filled circles) and LTE (open circles) for the stars with  $\log g \leq 3$  and triangles for  $\log g > 3$  Pb/Eu abundance ratios as a function of metallicity. The solid line indicates the Solar system meteoritic value. The two dotted lines correspond to a pure r-process production of Pb and Eu predicted by the waiting-point r-process model for a newly born (the low-lying curve) and 13 Gyr old (the up-lying curve) star as given by Roederer et al. (2009). The non-LTE abundances were calculated with  $S_H = 0.1$ .

The non-LTE and LTE Pb/Eu abundance ratios are plotted in Fig. 5. As shown by Hill et al. (2002) for CS 31082-001 and Frebel et al. (2007) for HE 1523-0901, the heavy elements beyond the iron group in these stars originate from the r-process, and the observed element abundance ratios can be used to test theoretical nucleosynthesis models. We found that both stars have very similar Pb/Eu abundance ratios at  $\log \varepsilon_{\text{NLTE}}(\text{Pb}/\text{Eu}) = 0.67$  and  $0.68$ , respectively, and that the WP r-process model for a 13 Gyr old star (Kratz et al. 2007, Roederer et al. 2009) perfectly reproduces the observations. We also stress that the Pb/Eu abundance ratios of the r-II stars match the Solar r-process ratio  $\log \varepsilon_{\text{SSr}}(\text{Pb}/\text{Eu}) = 0.82$  within the error bars. According to Plez et al. (2004), the uncertainty in the Pb abundance of CS 31082-001 is 0.15 dex. This provides strong evidence for universal Eu and Pb relative r-process yields during the Galactic history.

Despite the large scatter in the abundances, a clear upward trend is seen in the  $\log \varepsilon(\text{Pb}/\text{Eu}) - [\text{Fe}/\text{H}]$  plane for all stars with  $[\text{Fe}/\text{H}] > -2.3$ . The Pb/Eu abundance ratio grows from  $\log \varepsilon_{\text{NLTE}}(\text{Pb}/\text{Eu}) \approx 0.8$  at  $[\text{Fe}/\text{H}] = -2$  up to the solar value at  $[\text{Fe}/\text{H}] = -0.6$ . Following Roederer et al. (2010), we separated these stars in two groups depending on their metallicity. The low-metallicity sample (hereafter, LMS) includes 29 stars in the  $-2.26 \leq [\text{Fe}/\text{H}] < -1.40$  metallicity range, and the mildly metal-poor sample ( $-1.4 \leq [\text{Fe}/\text{H}] \leq -0.59$ , hereafter, MMPS) includes 21 stars. It is worth noting that each subsample is highly surface gravity biased due to a common selection effect. Namely, most LMS stars are cool giants, while the MMPS stars are mainly dwarf stars.

As seen in Fig. 5, the LMS stars have significantly higher Pb/Eu ratios compared to that of the r-II stars, independent of either LTE or non-LTE. Excluding a clear outlier, i.e., the star HD 108317 ( $[\text{Fe}/\text{H}] = -2.18$ ,  $\log \varepsilon_{\text{NLTE}}(\text{Pb}/\text{Eu}) = 1.91$ ), we calculated the mean  $\log \varepsilon_{\text{LTE}}(\text{Pb}/\text{Eu}) = 0.93 \pm 0.23$  and  $\log \varepsilon_{\text{NLTE}}(\text{Pb}/\text{Eu}) = 1.19 \pm 0.24$  from the 28 LMS stars. We shall conclude that the s-process in AGB stars started to produce lead before the Galactic metallicity grew to  $[\text{Fe}/\text{H}] = -2.3$ . The low-

metallicity s-process nucleosynthesis calculations (Roederer et al. 2010, Lugaro et al. 2011) do not contradict this observational finding. Roederer et al. (2010) presented the surface composition at the end of the AGB phase for a number of intermediate-mass models with  $[\text{Fe}/\text{H}] = -2.3$  and  $M = 4.5 - 6 M_{\odot}$ . The minimum value produced by those models is  $\log \varepsilon(\text{Pb}/\text{Eu}) = 1.9$ . Given sufficient time, their contributions could result in raising the Galactic Pb/Eu abundance ratio above the pure r-process one. Earlier, from analyses of the stellar (Ba, La, Nd)/(Eu, Dy) abundance ratios, Burris et al. (2000) and Simmerer et al. (2004) obtained evidences for that the s-process might be active as early as  $[\text{Fe}/\text{H}] = -2.3$  and  $-2.6$ , respectively.

For the MMPS stars, the obtained mean,  $\log \varepsilon_{\text{NLTE}}(\text{Pb}/\text{Eu}) = 1.58 \pm 0.31$ , is very close to the Solar System value,  $\log \varepsilon_{\text{met}}(\text{Pb}/\text{Eu}) = 1.53$  (Lodders et al. 2009). This supports the theoretical result of Travaglio et al. (2001) who predicted that the AGB stars with  $[\text{Fe}/\text{H}] \approx -1$  made the greatest contribution to the solar abundance of s-nuclei of lead. It is worth noting that LTE leads to 0.22 dex lower Pb/Eu abundance ratio for the MMPS stars. The star G 58-25, with  $[\text{Fe}/\text{H}] = -1.40$  and  $\log \varepsilon_{\text{NLTE}}(\text{Pb}/\text{Eu}) = 2.28$ , was not included in the mean calculations.

Generally, our findings are stable with respect to a variation in the stellar parameters that correspond to reasonable observational uncertainties and a variation in the  $S_H$  value. For example, for CS 31082-001, a change of +100 K in  $T_{\text{eff}}$  (a  $\sim 2\sigma$  error in Hill et al. (2002)) produces a change in the calculated Pb non-LTE abundance of +0.16 dex. Pb I 4057 Å is insensitive to a variation in  $\log g$  and microturbulence velocity,  $V_{\text{mic}}$ . The total effect of varying  $T_{\text{eff}}$ ,  $\log g$  (by +0.3 dex), and  $V_{\text{mic}}$  (by +0.2 km s<sup>-1</sup>) on the derived Eu abundance was estimated by Hill et al. (2002) as to be +0.12 dex. Thus, the Pb/Eu abundance ratio is only slightly affected by the uncertainties in stellar parameters. The non-LTE calculations performed for CS 31082-001 with  $S_H = 0$  and 1 result in only 0.04 and 0.02 dex lower  $\log \varepsilon(\text{Pb}/\text{Eu})$  values compared to that for  $S_H = 0.1$ . To evaluate the uncertainty in the Pb/Eu abundance ratios of the LMS and MMPS stars, we chosen the two representative stars HD 3008 (4250/0.25/-2.08) and G 102-020 (5250/4.44/-1.25). Simmerer et al. (2004) estimated that the stellar parameters of their sample are internally consistent to  $\Delta T_{\text{eff}} = 100$  K,  $\Delta \log g = 0.25$ , and  $\Delta V_{\text{mic}} = 0.1$  km s<sup>-1</sup>. An upward revision of the stellar parameters for HD 3008 results in a cumulative change of +0.11 dex in  $\log \varepsilon_{\text{Pb}}$  and +0.10 dex in  $\log \varepsilon_{\text{Eu}}$ . For G 102-020, the abundance errors caused by the uncertainties in the stellar parameters also have a common sign for Pb and Eu and amount to 0.09 and 0.06 dex, respectively.

We note that we have not considered effects on the abundances as a result of using 3D hydrodynamical model atmospheres. However, those effects were estimated for Pb I 4057 Å ( $E_{\text{exc}} = 1.32$  eV) and the Eu II lines arising from the ground state using the 3D-1D LTE abundance corrections calculated by Collet et al. (2007) and Hayek et al. (2011) for a sample of “fictitious” atomic (Na I, Mg I, Ca I, Fe I, and Fe II) lines at selected wavelengths, with varying lower-level excitation potentials and line strengths. Overall, 3D-1D corrections are negative for the lines of neutral atoms and decrease in absolute value with increasing  $E_{\text{exc}}$ . In the 4717/2.2/-1 models, they have similar values for all the chemical species, i.e., 3D-1D varies between -0.20 and -0.28 dex for the lines with  $E_{\text{exc}} = 0$  and between -0.10 and -0.18 dex for  $E_{\text{exc}} = 2$  eV. The 3D effects grow toward lower metallicity, however, with different rate for different atoms. In the 4732/2.2/-2 and 4858/2.2/-3 models, the 3D-1D corrections are similar for Mg I and Fe I, but different from

that for Na I and Ca I. For the weak Na I line with  $E_{\text{exc}} = 1.3$  eV and an equivalent width of  $\text{EW} < 20$  mÅ, 3D-1D  $\approx -0.12$  dex in the  $-3 \leq [\text{Fe}/\text{H}] \leq -1$  metallicity range. For the weak Fe I line with the same excitation potential, 3D-1D  $\approx -0.4, -0.3$ , and  $-0.17$  dex in the  $[\text{Fe}/\text{H}] = -3, -2$ , and  $-1$  model, respectively. The 3D effects are overall weak for the Fe II lines arising from the ground state. For example, for the moderate strength line ( $\text{EW} \approx 50$  mÅ), 3D-1D =  $-0.03, +0.15$ , and  $+0.15$  dex in the  $[\text{Fe}/\text{H}] = -3, -2$ , and  $-1$  model, respectively. We assume that 3D-1D corrections for the investigated Eu II lines are similar to that for the “fictitious” Fe II line with  $E_{\text{exc}} = 0$  eV. The 3D-1D correction for Pb I 4057 Å lies, probably, between those for Na I and Fe I. In case it is as large as that for Na I, accounting for the 3D effects results in approximately 0.1 dex lower Pb/Eu abundance ratio for the two r-II stars and 0.25 dex lower Pb/Eu value for the low-metallicity and mildly metal-poor samples. With such changes, our conclusions remain valid. If the 3D-1D correction for Pb I 4057 Å is as large as that for Fe I, the mean Pb/Eu abundance ratios of the r-II stars and the LMS stars are expected to be approximately 0.4 dex lower compared with the corresponding NLTE+1D values. However, in this case, it would be hard to understand why the Pb/Eu abundance ratio of the strongly r-process enhanced stars is significantly lower (by 0.5 dex) compared with the Solar System r-process value.

We note here that full 3D non-LTE computations have so far only been performed for Li I in the Sun and metal-poor stars (Asplund et al. 2003, Barklem et al. 2003, Cayrel et al. 2007, Sbordone et al. 2010) and for O I in the Sun (Asplund et al. 2004). It was found that the 3D+non-LTE effects are overall small for the Li I resonance line because the line strengthening due to the cooler temperatures in the upper atmospheric layers of the 3D model on the one hand, and line weakening from increased overionization on the other hand, largely cancel each other out. For O I, the non-LTE abundance corrections turned out similar in the 3D and 1D solar model atmospheres. In contrast, Shchukina et al. (2005) predicted stronger non-LTE effects for Fe I in 3D than in the 1D model, based on their 1.5D+non-LTE calculations for the Sun and HD 140283 (5700/3.7/−2.5). Full 3D non-LTE computations need to be done for Pb I to decide what is a difference in Pb/Eu abundance ratio between 3D+non-LTE and 1D+non-LTE cases and how this might affect our conclusions.

## 5. Non-LTE calculations for Th II

### 5.1. Thorium model atom

**Energy levels.** In the range of stellar parameters that we are considering here, the majority of the element exists as Th II. For example, the fraction of neutral thorium, with its ionization energy  $\chi_{\text{ion}} = 6.3$  eV, does not exceed  $10^{-3}$  throughout the 4500/1/−3 atmosphere and  $6 \cdot 10^{-3}$  throughout the solar atmosphere. We thus neglected Th I when constructing the model atom. The Th II term structure is produced by multiple electronic configurations (see Fig. 6) and consists of thousands energy levels. The ground configuration is  $6d^2 7s$ . We used the energy levels with  $E_{\text{exc}} \leq 6.88$  eV, which amount to 416 levels from Blaise & Wyart (1992). The higher excitation levels play a minor role in the population and depopulation of Th II, because the next ionization stage, Th III, represents a minor fraction of the thorium abundance. For example, the contribution of Th III to thorium abundance is smaller than 0.2 / 1.5 % in the cool VMP / solar models outside  $\log \tau_{5000} = 0$ . The levels with common parity and close energies were combined whenever the energy separation

is smaller than 0.01 eV at  $E_{\text{exc}} < 4$  eV and smaller than 0.1 eV at higher  $E_{\text{exc}}$ . The final model atom includes 184 levels of Th II (Fig. 6).

The Th III ground state  $5f6d^3 H_4^0$  is a poor representation of the Th III ionization stage. The odd  $5f6d$  and  $5f7s$  and the even  $6d^2$  and  $6d7s$  configurations of Th III produce many low-excitation levels. The energy of  $6d^2 \ ^3F_2$ ,  $E_{\text{exc}} = 63.2$  cm $^{-1}$ , is the smallest distance between the lowest levels of both parities ever found in an atomic spectrum. As a result, the Th III partition function ( $U$ ) is significantly larger compared with the statistical weight  $g = 9$  of the ground state. For example,  $U(\text{Th III}) = 49.14$  at the temperature  $T = 4990$  K and grows to  $U(\text{Th III}) = 81.11$  at  $T = 8318$  K. These values were computed using the Th III energy levels from Blaise & Wyart (1992). Assuming that the low-excitation levels of Th III are thermally coupled to the ground state, we included Th III in the model atom as a single state with  $g = 49$ , while keeping the energy of the ground state.

**Radiative rates.** Accurate  $gf$ -values based on measured natural radiative lifetimes and branching ratios were obtained by Nilsson et al. (2002) for 180 transitions between the lowest ( $E_{\text{exc}} = 0 - 2.25$  eV) even parity levels of the  $6d^2 7s$ ,  $6d7s^2$ , and  $6d^3$  electronic configurations and the intermediate energy ( $E_{\text{exc}} = 2.26 - 4.08$  eV) odd parity levels. For another 1244 transitions, we used  $gf$ -values of Kurucz & Bell (1995) which are accessible via the VALD database (Kupka et al. 1999). These two sources provide the data for 955  $b - b$  transitions between combined levels in our model atom. They all were included in SE calculations. We refer to this atomic model as Th-1.

The second atomic model, Th-2, includes the extended system of  $b - b$  radiative transitions. We estimated the total number of allowed transitions in the system of 416 Th II levels assuming that every transition between the different parity levels with  $\Delta J = 0, \pm 1$  is an allowed one. The exception are the  $J = 0 \leftrightarrow J = 0$  transitions. This gives 20 214 transitions, and for 18 790 of them, oscillator strengths ( $f_{ij}$ ) are missing. The 1 562 of the latter transitions, with the energy separation of less than 0.25 eV, were treated as forbidden ones because of insignificant contribution of the radiative to the total transition rate, irrespective of the transition  $gf$ -value. For every of the remaining 17 228 transitions,  $f_{ij} = 10^{-4}$  was adopted. Such a choice was based on the inspection of the known  $gf$ -values for Th II. No transition from the Nilsson et al. (2002) and Kurucz & Bell (1995) data sets has  $f_{ij} \leq 10^{-4}$ . In this atomic model, the 5 661  $b - b$  transitions were included in SE calculations.

The photoionization cross-sections were computed using the hydrogen approximation formula with  $n = n_{\text{eff}}$ , because no accurate data is available for the Th II levels.

**Collisional rates.** The same formulas as for Pb I were employed for the transitions in Th II, with  $\Upsilon = 2$  for the forbidden ones.

### 5.2. Departures from LTE for Th II

The non-LTE calculations for Th II were performed with the MARCS solar model atmosphere and with the models representing the atmospheres of VMP stars with  $[\text{Fe}/\text{H}] = -2$  and  $-3$  (see Table 3). Figure 7 shows the departure coefficients of the selected Th II levels in the 5780/4.44/0 and 4500/1.0/−3 models. We found that the lowest 72 levels, i.e., up to the level denoted as 726d ( $E_{\text{exc}} = 2.46$  eV), keep nearly TE populations ( $b \approx 1$ ) in the atmosphere inside  $\log \tau_{5000} = -2$  and  $-1$  for the solar and VMP models, respectively. For all the higher excitation levels,  $b > 1$ . This is because the population of the odd parity  $5f6d^2$  and  $6d7s7p$  levels with  $E_{\text{exc}} = 3 - 4.8$  eV is controlled



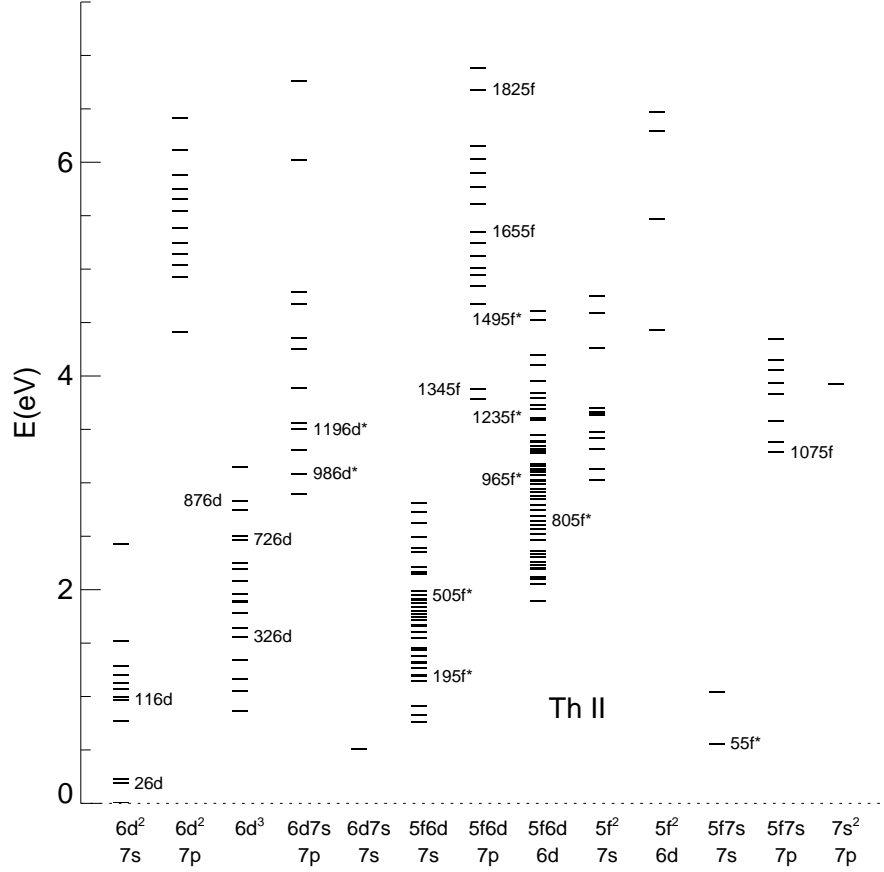


**Fig. 6.** Model atom of Th II. The names of the levels important for understanding the non-LTE mechanisms are indicated.

by the strong radiative transitions from the three lowest  $6d^27s$  states and the  $6d7s^2$  level, such as  $6d^27s^4F_{3/2} - 6d7s7p$  ( $E_{\text{exc}} = 3.084$  eV,  $J = 5/2$ ) denoted in our model atom as  $16d - 986d^*$  and producing the line at  $4019 \text{ \AA}$ ,  $16d - 965f^*$  ( $4094 \text{ \AA}$ ),  $26d - 1196d^*$  ( $3741 \text{ \AA}$ ), and  $36d - 1495f^*$  ( $2895 \text{ \AA}$ ). These transitions are pumped by the ultraviolet  $J_{\nu} - B_{\nu}(T_e)$  excess radiation and produce enhanced excitation of the upper levels far inside the atmosphere. This overpopulation is redistributed to the even parity high excitation levels through inelastic collisions.

The Th-2 atomic model includes more pumping transitions compared to the Th-1 one, and the departures from LTE are expected to be stronger when using the Th-2 model. We checked the populations of the lower and upper levels of the Th II  $4019 \text{ \AA}$  transition. In the line formation layers, around  $\log \tau_{5000} = -0.45$  and  $-0.55$  in the solar and  $4500/1.0/-3$  models, respectively, the difference in non-LTE populations between the Th-2 and Th-1 atomic models is negligible for the Th II ground state. This is easy to understand because the lowest Th II levels contain the majority of the element, and no mechanism is able to significantly change their populations compared to the TE ones. For the upper level,  $986d^*$ , a small difference of 3 % between using Th-2 and Th-1 was found in the VMP model, and very similar populations were obtained in the solar model.

The Th II lines used in abundance analyses all arise from either the ground state or low-excitation levels with  $E_{\text{exc}} \leq$

$0.51$  eV, for which  $b \approx 1$  holds in the line formation layers (Fig. 7). Nevertheless, for each line, non-LTE leads to its weakening compared to the LTE strength, owing to the overpopulation of the upper level relative to the TE population that results in  $b_u/b_l > 1$  and the rise of the line source function above the Planck function in the line-formation layers. Overall, the obtained non-LTE abundance corrections are positive. For the Sun, the departures from LTE are small irrespective of the applied  $S_H$  value, such that  $\Delta_{\text{NLTE}}(\text{Th II } 4019 \text{ \AA}) = 0.06$  and  $0.00$  dex in case of  $S_H = 0$  and  $1$ , respectively. In the VMP models, the non-LTE correction is very sensitive to treatment of inelastic collisions with H I atoms. For example, for  $4500/1/-3$ , it amounts to  $\Delta_{\text{NLTE}} = +0.52$  dex in the calculations with pure electronic collisions and it varies between  $\Delta_{\text{NLTE}} = +0.12$  and  $+0.03$  dex when collisions with H I atoms are taken into account with  $S_H = 0.1$  to  $1$ . The use of the Th-1 atomic model results in  $0.01$  dex smaller non-LTE corrections.

Table 3 presents  $\Delta_{\text{NLTE}}$  for the two lines, Th II  $4019$  and  $4086 \text{ \AA}$ , from the calculations with the Th-2 atomic model and  $S_H = 0.1$ . For a given  $T_{\text{eff}}$ , the departures from LTE grow toward lower surface gravity due to decreasing contribution of the collisional to the total transition rates. Maximum  $\Delta_{\text{NLTE}}$  were calculated for the  $4000/0.0/-2$  model, and they amount to  $+0.21$  dex for Th II  $4019 \text{ \AA}$  and  $+0.14$  dex for Th II  $4086 \text{ \AA}$ . The metallicity effect is less pronounced in Table 3 because, for the  $[\text{Fe}/\text{H}] = -3$

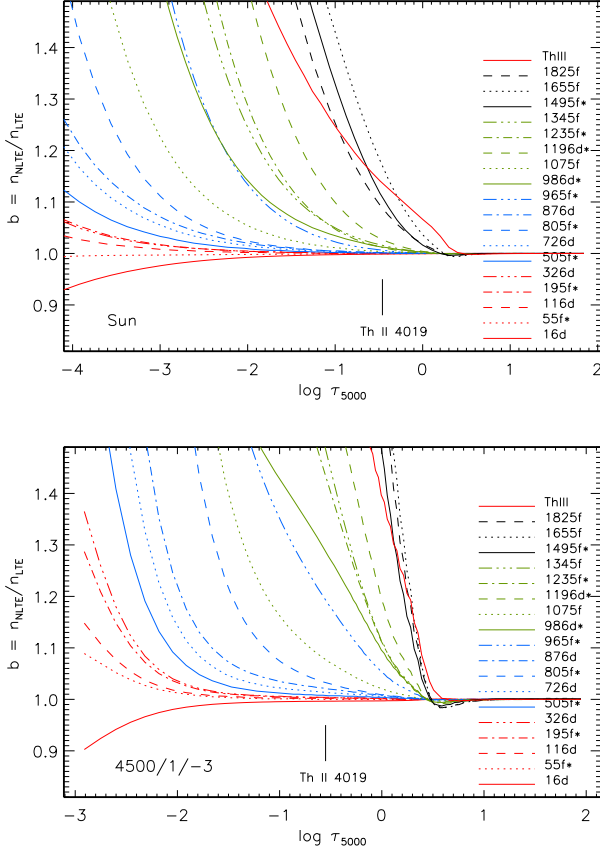


**Fig. 7.** The same as in Fig. 3 for the selected levels of Th II and the Th III ground state from the calculations with the Th-2 atomic model. The vertical lines indicate the locations of line core formation depths for Th II 4019.

models, the non-LTE calculations were performed with a higher Th abundance compared with that in the  $[\text{Fe}/\text{H}] = -2$  models.

## 6. Conclusions

We built a comprehensive model atom for neutral lead using atomic data for the energy levels and transition probabilities from laboratory measurements and theoretical predictions. The non-LTE calculations for Pb I were performed for the first time for the Sun and for a set of stellar parameters characteristic of metal-poor stars in the  $-2.95 \leq [\text{Fe}/\text{H}] \leq -0.59$  metallicity range. We found that the main non-LTE mechanism for Pb I is the ultraviolet overionization, although radiative pumping of the strong transitions arising from the low-lying levels tends to produce enhanced excitation of the Pb I levels with  $E_{\text{exc}} > 4$  eV. Overall, non-LTE leads to weakened Pb I lines and positive non-LTE abundance corrections. The departures from LTE grow with decreasing metallicity and, for a given metallicity, increase toward higher effective temperatures and lower surface gravities. The main source of the uncertainty in the calculated non-LTE abundance corrections are poorly known inelastic collisions with H I atoms. From analysis of either solar or stellar Pb I lines we can not empirically constrain their efficiency in SE calculations. With  $S_{\text{H}} = 0.1$ , chosen based on our estimates for Ca I-Ca II and Fe I-Fe II (Mashonkina et al. 2007, 2011),  $\Delta_{\text{NLTE}}$  of Pb I 4057 Å ranges between 0.16 dex in the solar model and 0.56 dex in the 4825/1.5/-2.9 model.

**Table 3.** Non-LTE abundance corrections (dex) for the Th II lines from the calculations with  $S_{\text{H}} = 0.1$ .

$T_{\text{eff}}$	$\log g$	$[\text{Fe}/\text{H}]$	$[\text{Th}/\text{Fe}]^1$	$\Delta_{\text{NLTE}}$	
				4019 Å	4086 Å
5780	4.44	0	0.09 <sup>2</sup>	0.01	- <sup>3</sup>
4000	0.0	-2	0.4	0.21	0.14
4000	0.5	-2	0.4	0.13	0.08
4250	0.5	-2	0.4	0.16	0.09
4250	1.0	-2	0.4	0.10	0.06
4500	1.0	-2	0.4	0.12	0.07
4500	1.5	-2	0.4	0.07	0.04
4750	1.5	-2	0.4	0.09	0.05
4750	2.0	-2	0.4	0.06	0.03
5250	2.5	-2	0.4	0.05	-
4500	1.0	-3	1.75	0.12	0.06
4500	1.5	-3	1.75	0.07	0.03
4750	1.0	-3	1.75	0.15	0.09
4750	1.5	-3	1.75	0.09	0.05

<sup>1</sup> Thorium abundance used in non-LTE calculations

<sup>2</sup> Absolute thorium abundance,  $\log \varepsilon_{\text{Th}}$

<sup>3</sup> Calculated equivalent width is smaller than 1 mÅ

We also built a model atom for singly-ionized thorium using atomic data for the energy levels from laboratory measurements. The non-LTE calculations for Th II were performed for the first time for the Sun and for the small grid of model atmospheres with  $[\text{Fe}/\text{H}] = -2$  and  $-3$ . In contrast to Pb I, Th II is the majority species in the stellar parameter range that we have covered, and the main non-LTE mechanism for Th II is connected to the pumping transitions arising from the low-excitation levels, with  $E_{\text{exc}} < 1$  eV. Overall, non-LTE leads to weakened Th II lines and positive non-LTE abundance corrections. Compared with Pb I, the departures from LTE for Th II are even more sensitive to the efficiency of collisions with H I atoms. With  $S_{\text{H}} = 0.1$ ,  $\Delta_{\text{NLTE}}$  of the investigated Th II lines nowhere exceeds 0.21 dex.

We caution against using the LTE assumption in stellar analyses of Pb abundance and also the elemental abundance ratios involving Pb and some other element observed in the lines of their majority species, such as Eu, Th, or U.

Taking advantage of our SE approach for Pb I, we obtained good agreement, within 0.03 dex, between meteoritic and absolute solar abundances from the calculations with the Holweger & Mueller (1974) solar model atmosphere and  $S_{\text{H}} = 0.1$ . Our final value is  $\log \varepsilon_{\text{Pb},\odot} = 2.09$ .

We then calculated the non-LTE abundances of Pb and Eu for the Roederer et al. (2010) metal-poor stars and complemented that sample with HE 1523-0901 (Frebel et al. 2007) and HD 29907 (Sitnova & Mashonkina 2011). We found that the two strongly r-process enhanced (r-II) stars have very similar Pb/Eu abundance ratios, with the mean  $\log \varepsilon_{\text{NLTE}}(\text{Pb}/\text{Eu}) = 0.68 \pm 0.01$ , and the waiting-point r-process model as presented by Roederer et al. (2009) reproduces the observations very well. The revised Pb/Eu abundance ratios of the r-II stars match, within the error bars, the corresponding solar r-process ratio. Thus, *the universality of the r-process was proved* not only for the second r-process peak elements from Ba to Hf as found earlier by Sneden et al. (1996), Hill et al. (2002), Sneden et al. (2008, and references therein), but also for the heavier element Pb.

It was found that the stars in the  $-2.3 \leq [\text{Fe}/\text{H}] < -0.6$  metallicity range, reveal a clear upward trend in the  $\log \varepsilon(\text{Pb}/\text{Eu}) - [\text{Fe}/\text{H}]$  plane. Following Roederer et al. (2010), we separated

these stars in two groups depending on their metallicity. The lower metallicity stars ( $[\text{Fe}/\text{H}] < -1.4$ ) turned out to have, on average, 0.51 dex higher Pb/Eu ratios compared with that of the r-II stars. This led us to conclude that *the s-process production of lead started before the Galactic metallicity grew to*  $[\text{Fe}/\text{H}] = -2.3$ . It is worth noting that the studies of Burris et al. (2000) and Simmerer et al. (2004) who obtained (Ba, La, Nd)/(Eu, Dy) abundance ratios of metal-poor stars, also found that the s-process has been active as early as  $[\text{Fe}/\text{H}] = -2.3$  and  $-2.6$ , respectively.

The mean,  $\log \varepsilon_{\text{NLTE}}(\text{Pb}/\text{Eu}) = 1.58 \pm 0.31$ , for the mildly metal-poor subsample ( $-1.4 \leq [\text{Fe}/\text{H}] \leq -0.59$ ) turned out *very close to the Solar System value*,  $\log \varepsilon_{\text{met}}(\text{Pb}/\text{Eu}) = 1.53$  (Lodders et al. 2009). This is in agreement with the theoretical result of Travaglio et al. (2001) who predicted that the AGB stars with  $[\text{Fe}/\text{H}] \simeq -1$  made the greatest contribution to the abundance of s-nuclei of lead in the presolar nebula from which the Sun originated.

**Acknowledgements.** L.M. is supported by the Swiss National Science Foundation (SCOPE project No. IZ73Z0-128180/1) and the RF President with a grant on Leading Scientific Schools 3602.2012.2. A. F. is, in part, supported by a Clay Fellowship administered by the Smithsonian Astrophysical Observatory. We used the MARCS model atmosphere library and the NIST and VALD databases.

## References

- Ahad, A., Nadeem, A., Bhatti, S. A., & Baig, M. A. 2005, *European Physical Journal D*, 32, 271
- Anders, E. & Grevesse, N. 1989, *Geochim. Cosmochim. Acta*, 53, 197
- Asplund, M., Carlsson, M., & Botnen, A. V. 2003, *A&A*, 399, L31
- Asplund, M., Grevesse, N., Sauval, A. J., Allende Prieto, C., & Kiselman, D. 2004, *A&A*, 417, 751
- Asplund, M., Grevesse, N., Sauval, A. J., & Scott, P. 2009, *ARA&A*, 47, 481
- Barklem, P. S., Belyaev, A. K., & Asplund, M. 2003, *A&A*, 409, L1
- Barklem, P. S., Belyaev, A. K., Guitou, M., et al. 2011, *A&A*, 530, A94
- Biémont, E., Garnir, H. P., Palmeri, P., Li, Z. S., & Svanberg, S. 2000, *MNRAS*, 312, 116
- Blaise, J. & Wyart, J. F. 1992, *Energy levels and atomic spectra of actinides*, International tables of selected constants. (The French Centre National de la Recherche Scientifique and Belgian Government)
- Brault, J., Testerman, L., & Observatory, K. P. N. 1972, *Kitt Peak Solar Atlas: 2942 - 10800 Å* (Kitt Peak National Observatory)
- Brown, C. M., Tilford, S. G., & Ginter, M. L. 1977, *Journal of the Optical Society of America* (1917-1983), 67, 1240
- Burris, D. L., Pilachowski, C. A., Armandroff, T. E., et al. 2000, *ApJ*, 544, 302
- Butler, K. & Giddings, J. 1985, *Newsletter on the analysis of astronomical spectra*, No. 9, University of London
- Cayrel, R., Hill, V., Beers, T. C., et al. 2001, *Nature*, 409, 691
- Cayrel, R., Steffen, M., Chand, H., et al. 2007, *A&A*, 473, L37
- Christlieb, N., Beers, T. C., Barklem, P. S., et al. 2004, *A&A*, 428, 1027
- Collet, R., Asplund, M., & Trampedach, R. 2007, *A&A*, 469, 687
- Cowan, J. J. & Thielemann, F.-K. 2004, *Physics Today*, 57, 47
- Cowan, R. D. 1981, *The Theory of Atomic Structure and Spectra* (Univ. of California Press, Berkeley, California, USA)
- Dembczyński, J., Stachowska, E., Wilson, M., Buch, P., & Ertmer, W. 1994, *Phys. Rev. A*, 49, 745
- Drawin, H.-W. 1961, *Zeitschrift für Physik*, 164, 513
- Frebel, A., Christlieb, N., Norris, J. E., et al. 2007, *ApJ*, 660, L117
- Fuhr, J. R. & Wiese, W. L. 1992, *NIST Atomic Transition Probability Tables*, CRC Handbook of Chemistry & Physics, 77th Edition, D. R. Lide (CRC Press, Inc., Boca Raton, FL)
- Gallino, R., Arlandini, C., Busso, M., et al. 1998, *ApJ*, 497, 388
- Gustafsson, B., Edvardsson, B., Eriksson, K., et al. 2008, *A&A*, 486, 951
- Hasegawa, S. & Suzuki, A. 1996, *Phys. Rev. A*, 53, 3014
- Hayek, W., Asplund, M., Collet, R., & Nordlund, Å. 2011, *A&A*, 529, A158
- Heppinstall, R. & Marr, G. V. 1969, *Proc. Roy. Soc. A*, 310, 35
- Hill, V., Plez, B., Cayrel, R., et al. 2002, *A&A*, 387, 560
- Hillebrandt, W. 1978, *Space Sci. Rev.*, 21, 639
- Holweger, H. & Mueller, E. A. 1974, *Sol. Phys.*, 39, 19
- Ivans, I. I., Sneden, C., Gallino, R., Cowan, J. J., & Preston, G. W. 2005, *ApJ*, 627, L145
- Kratz, K.-L., Farouqi, K., Pfeiffer, B., et al. 2007, *ApJ*, 662, 39
- Krause, M. O., Gerard, P., & Fahlman, A. 1986, *Phys. Rev. A*, 34, 4511
- Kupka, F., Piskunov, N., Ryabchikova, T. A., Stempels, H. C., & Weiss, W. W. 1999, *A&AS*, 138, 119
- Kurucz, R. L. 1994, *SYNTHES Spectrum Synthesis Programs and Line Data*, CD-ROM No. 18 (Cambridge, Mass)
- Kurucz, R. L. & Bell, B. 1995, *Atomic Line Data*, CD-ROM No. 23 (<http://kurucz.harvard.edu>)
- Li, Z. S., Zhankui, J., Berzinsh, U., Persson, A., & Svanberg, S. 2001, *Journal of Physics B Atomic Molecular Physics*, 34, 3501
- Lodders, K., Plame, H., & Gail, H.-P. 2009, in *Landolt-Börnstein - Group VI Astronomy and Astrophysics Numerical Data and Functional Relationships in Science and Technology Volume 4B: Solar System*. Edited by J.E. Trümper, 2009, 4.4., 44–54
- Lugaro, M., Karakas, A. I., Stancliffe, R. J., & Rijs, C. 2011, *ArXiv e-prints*, 1112.2757
- Mashonkina, L. & Gehren, T. 2000, *A&A*, 364, 249
- Mashonkina, L., Gehren, T., Shi, J.-R., Korn, A. J., & Grupp, F. 2011, *A&A*, 528, A87
- Mashonkina, L., Korn, A. J., & Przybilla, N. 2007, *A&A*, 461, 261
- Mihalas, D. 1978, *Stellar atmospheres /2nd edition/* (San Francisco, W. H. Freeman and Co.)
- Moore, C. E. 1958, *Atomic Energy Levels*, Nat.Bur.Stand. (U.S.) Circ. No.467, V.III (Nat.Bur.Stand. (U.S.))
- Müller, M., Bowering, N., Schäfers, F., & Heinzmann, U. 1990, *Phys. Scr*, 41, 38
- Nilsson, H., Zhang, Z. G., Lundberg, H., Johansson, S., & Nordström, B. 2002, *A&A*, 382, 368
- Plez, B., Hill, V., Cayrel, R., et al. 2004, *A&A*, 428, L9
- Reetz, J. K. 1991, *Diploma Thesis* (Universität München)
- Roederer, I. U., Cowan, J. J., Karakas, A. I., et al. 2010, *ApJ*, 724, 975
- Roederer, I. U., Kratz, K.-L., Frebel, A., et al. 2009, *ApJ*, 698, 1963
- Rybicki, G. B. & Hummer, D. G. 1991, *A&A*, 245, 171
- Rybicki, G. B. & Hummer, D. G. 1992, *A&A*, 262, 209
- Sbordone, L., Bonifacio, P., Caffau, E., et al. 2010, *A&A*, 522, A26
- Shchukina, N. G., Trujillo Bueno, J., & Asplund, M. 2005, *ApJ*, 618, 939
- Simmerer, J., Sneden, C., Cowan, J. J., et al. 2004, *ApJ*, 617, 1091
- Sitnova, T. M. & Mashonkina, L. I. 2011, *Astronomy Letters*, 37, 480
- Sneden, C., Cowan, J. J., & Gallino, R. 2008, *ARA&A*, 46, 241
- Sneden, C., McWilliam, A., Preston, G. W., et al. 1996, *ApJ*, 467, 819
- Steenbock, W. & Holweger, H. 1984, *A&A*, 130, 319
- Takeda, Y. 1995, *PASJ*, 47, 463
- Travaglio, C., Galli, D., Gallino, R., et al. 1999, *ApJ*, 521, 691
- Travaglio, C., Gallino, R., Busso, M., & Gratton, R. 2001, *ApJ*, 549, 346
- van Regemorter, H. 1962, *ApJ*, 136, 906
- Wood, D. R. & Andrew, K. L. 1968, *Journal of the Optical Society of America* (1917-1983), 58, 818



**Table 2.** Non-LTE and LTE abundances of Pb and Eu and non-LTE abundance corrections (dex) for the Pb I 4057 Å and Eu II 4129 Å lines in the Roederer et al. (2010) stellar sample.

Star	$T_{\text{eff}}$	$\log g$	[Fe/H]	Pb			Eu		
				$\log \epsilon_{\text{NLTE}}^{\text{I}}$	$\log \epsilon_{\text{LTE}}$	$\Delta_{\text{NLTE}}^{\text{I}}$	$\log \epsilon_{\text{NLTE}}^{\text{I}}$	$\log \epsilon_{\text{LTE}}$	$\Delta_{\text{NLTE}}^{\text{I}}$
BD+01 2916	4200	0.40	-1.92	0.12	-0.20	0.32	-1.14	-1.22	0.08
BD+19 1185	5500	4.19	-1.09	1.06	0.77	0.29	-0.18	-0.23	0.05
BD+29 2356	4760	1.60	-1.59	0.65	0.35	0.30	-0.62	-0.69	0.07
BD+30 2611	4330	0.60	-1.50	0.92	0.56	0.36	-0.29	-0.36	0.07
CS31082-001	4825	1.50	-2.90	0.01	-0.55	0.56	-0.66	-0.72	0.06
G009-036	5625	4.57	-1.17	1.53	1.25	0.28	-0.11	-0.16	0.05
G028-043	5060	4.50	-1.64	0.97	0.69	0.28	-0.48	-0.53	0.05
G029-025	5225	4.28	-1.09	1.06	0.80	0.26	-0.18	-0.23	0.05
G058-025	6000	4.21	-1.40	1.67	1.29	0.38	-0.61	-0.66	0.05
G059-001	5920	3.98	-0.95	1.98	1.64	0.34	-0.24	-0.29	0.05
G068-003	4975	3.50	-0.76	1.49	1.19	0.30	0.22	0.16	0.06
G095-057A	4955	4.40	-1.22	1.35	1.14	0.21	-0.19	-0.23	0.04
G102-020	5250	4.44	-1.25	1.04	0.79	0.25	-0.27	-0.32	0.05
G102-027	5600	3.75	-0.59	1.87	1.64	0.23	0.43	0.40	0.03
G113-022	5525	4.25	-1.18	1.49	1.19	0.30	-0.08	-0.13	0.05
G122-051	4864	4.51	-1.43	0.54	0.34	0.20	-0.23	-0.27	0.04
G123-009	5490	4.75	-1.25	1.40	1.13	0.27	-0.16	-0.21	0.05
G126-036	5490	4.50	-1.06	1.94	1.67	0.27	0.09	0.04	0.05
G140-046	4980	4.42	-1.30	1.41	1.19	0.22	-0.37	-0.41	0.04
G179-022	5080	3.20	-1.35	0.72	0.39	0.33	-0.17	-0.22	0.05
G221-007	5020	3.37	-0.98	1.99	1.69	0.30	-0.06	-0.11	0.05
HD 3008	4250	0.25	-2.08	-0.21	-0.56	0.35	-1.02	-1.09	0.07
HD 6755	5100	2.93	-1.68	0.73	0.32	0.41	-0.44	-0.50	0.06
HD 6833	4400	1.50	-0.85	1.93	1.69	0.24	0.15	0.10	0.05
HD 8724	4535	1.40	-1.91	0.32	0.00	0.32	-0.80	-0.86	0.06
HD 23798	4450	1.06	-2.26	0.09	-0.21	0.30	-1.30	-1.36	0.06
HD 26297	4320	1.11	-1.98	0.22	-0.11	0.33	-1.16	-1.22	0.06
HD 29574	4250	0.80	-2.00	0.25	-0.06	0.31	-0.57	-0.63	0.06
HD 29907 <sup>2</sup>	5500	4.64	-1.55	1.03	0.70	0.33	-0.45	-0.50	0.05
HD 37828	4350	1.50	-1.62	1.14	0.77	0.37	-0.48	-0.53	0.05
HD 44007	4850	2.00	-1.72	0.67	0.31	0.36	-0.87	-0.94	0.07
HD 63791	4675	2.00	-1.90	0.58	0.22	0.36	-0.85	-0.92	0.07
HD 74462	4700	2.00	-1.52	0.79	0.49	0.30	-0.32	-0.39	0.07
HD 105755	5700	3.82	-0.83	1.71	1.43	0.28	0.07	0.02	0.05
HD 106516	6170	4.21	-0.81	1.85	1.56	0.29	0.05	-0.04	0.09
HD 108317	5234	2.68	-2.18	0.69	0.17	0.52	-1.22	-1.32	0.10
HD 121135	4934	1.91	-1.54	0.72	0.38	0.34	-0.63	-0.70	0.07
HD 122956	4508	1.55	-1.95	0.19	-0.13	0.32	-0.73	-0.79	0.06
HD 141531	4360	1.14	-1.79	0.52	0.20	0.32	-0.66	-0.72	0.06
HD 166161	5350	2.56	-1.23	1.19	0.84	0.35	-0.41	-0.48	0.07
HD 171496	4950	2.37	-0.67	1.60	1.41	0.19	0.17	0.11	0.06
HD 175305	4770	1.80	-1.73	0.06	-0.28	0.34	-0.82	-0.89	0.07
HD 187111	4270	1.05	-1.97	0.21	-0.10	0.31	-0.82	-0.88	0.06
HD 201891	5910	4.19	-1.09	1.58	1.25	0.33	-0.17	-0.22	0.05
HD 204543	4670	1.49	-1.87	0.41	0.05	0.36	-0.98	-1.05	0.07
HD 206739	4650	1.78	-1.72	0.69	0.38	0.31	-0.55	-0.62	0.07
HD 210295	4750	2.50	-1.46	1.04	0.72	0.32	-0.27	-0.34	0.07
HD 214925	4050	0.00	-2.08	-0.13	-0.50	0.37	-0.97	-1.09	0.12
HD 220838	4300	0.60	-1.80	0.39	0.05	0.34	-0.86	-0.93	0.07
HD 221170	4510	1.00	-2.16	0.21	-0.09	0.30	-0.80	-0.86	0.06
HD 235766	4650	1.20	-1.93	0.42	0.10	0.32	-0.80	-0.86	0.06
HE 1523-0901 <sup>3</sup>	4630	1.00	-2.95	0.11	-0.34 <sup>4</sup>	0.45	-0.57	-0.62	0.05

<sup>1</sup> from the calculations with  $S_{\text{H}} = 0.1$ ,<sup>2</sup> stellar parameters and LTE abundances from Sitnova & Mashonkina (2011),<sup>3</sup> stellar parameters and europium LTE abundance from Frebel et al. (2007),<sup>4</sup> Frebel et al. (2012, in preparation).